RIM-binding protein 2 regulates release probability by fine-tuning calcium channel localization at murine hippocampal synapses

M. Katharina Grauel[a,b,c,1], Marta Maglione[b,c,d,1], Suneel Reddy-Alla[b,c,1], Claudia G. Willmes[b,e,f], Marisa M. Brockmann[a,b], Thorsten Trimbuch[a,b], Tanja Rosenmund[a,b], Maria Pangalos[b,f], Gülçin Vardar[a,b], Alexander Stumpf[b,f], Alexander M. Walter[g], Benjamin R. Rost[b,f,h], Britta J. Eickholt[b,e], Volker Haucke[b,d,i], Dietmar Schmitz[b,f,h,2], Stephan J. Sigrist[b,c,2], and Christian Rosenmund[a,b,2]

[a]Institute of Neurophysiology, Charité Universitätsmedizin, 10117 Berlin, Germany; [b]NeuroCure Cluster of Excellence, Charité Universitätsmedizin, 10117 Berlin, Germany; [c]Institute of Biology, Department of Biology, Chemistry, Pharmacy, Freie Universität Berlin, 14195 Berlin, Germany; [d]Department of Molecular Pharmacology and Cell Biology, Leibniz Institut für Molekulare Pharmakologie (FMP), 13125 Berlin, Germany; [e]Institute of Biochemistry, Charité Universitätsmedizin, 10117 Berlin, Germany; [f]Neuroscience Research Center (NWFZ), Charité Universitätsmedizin, 10117 Berlin, Germany; [g]Molecular and Theoretical Neuroscience, Leibniz-Institut für Molekulare Pharmakologie, 10117 Berlin, Germany; [h]DZNE- German Center for Neurodegenerative Diseases, Charité Universitätsmedizin, 10117 Berlin, Germany; and [i]Institute of Chemistry and Biochemistry, Department of Biology, Chemistry, Pharmacy, Freie Universität Berlin, 14195 Berlin, Germany

Edited by Thomas C. Südhof, Stanford University School of Medicine, Stanford, CA, and approved August 15, 2016 (received for review March 31, 2016)

The tight spatial coupling of synaptic vesicles and voltage-gated Ca^{2+} channels (Ca_Vs) ensures efficient action potential-triggered neurotransmitter release from presynaptic active zones (AZs). Rab-interacting molecule-binding proteins (RIM-BPs) interact with Ca^{2+} channels and via RIM with other components of the release machinery. Although human RIM-BPs have been implicated in autism spectrum disorders, little is known about the role of mammalian RIM-BPs in synaptic transmission. We investigated RIM-BP2–deficient murine hippocampal neurons in cultures and slices. Short-term facilitation is significantly enhanced in both model systems. Detailed analysis in culture revealed a reduction in initial release probability, which presumably underlies the increased short-term facilitation. Superresolution microscopy revealed an impairment in $Ca_V2.1$ clustering at AZs, which likely alters Ca^{2+} nanodomains at release sites and thereby affects release probability. Additional deletion of RIM-BP1 does not exacerbate the phenotype, indicating that RIM-BP2 is the dominating RIM-BP isoform at these synapses.

RIM-BP2 | calcium channel coupling | release probability | short-term plasticity | active zone structure

At the presynapse, coupling between action potentials (APs) and synaptic vesicle fusion is exquisitely precise, ensuring high temporal fidelity of neuron-to-neuron signaling in the nervous system. Two properties are thought to be responsible for this remarkable precision: a highly efficient release apparatus that transduces Ca^{2+} signals into vesicle fusion and a tightly organized active zone (AZ), where the release apparatus and voltage-gated Ca^{2+} channels (Ca_Vs) are spatially coupled. Rab-interacting molecules (RIM) are thought to contribute to both properties, because loss of RIM impairs vesicle priming (1) and Ca_V localization at the AZ (2). RIM-binding proteins (RIM-BPs) directly interact with RIM (3), the pore-forming subunits of Ca_V1 and Ca_V2 channels (2, 4, 5), and Bassoon (5), and have therefore been suggested to play a role in presynaptic Ca_V localization. The *Drosophila* homolog of RIM-binding proteins (DRBP) is indeed crucial for neurotransmitter release at the AZ of neuromuscular junctions (NMJs) because loss of DRBP reduces Ca_V abundance and impairs the integrity of the AZ scaffold (6). DRBP-deficient flies show severe impairment of neurotransmitter release along with increased short-term facilitation (6, 7).

Recently, Acuna et al. (8) published a report on the combined loss of RIM-BP1 and RIM-BP2 in mouse synapses. The authors report that although RIM-BPs are not essential for synaptic transmission, AP-triggered neurotransmitter release is more variable and the sensitivity to the Ca^{2+} chelator EGTA is increased at the Calyx of Held, suggesting a larger coupling distance of Ca_V and the release machinery.

In the present study, we further investigated the consequences of constitutive deletion of RIM-BP2 on the structure and function of mouse hippocampal synapses. We show that loss of RIM-BP2 leads to a moderate reduction in initial release probability, which translates into profound changes in short-term plasticity (STP). This deficit can be overcome by increasing extracellular Ca^{2+}. We established triple-channel time-gated stimulated emission depletion (gSTED) microscopy for RIM-BP2, Munc13-1, and Bassoon, as well as for $Ca_V2.1$, RIM, and the postsynaptic marker protein Homer1. Using this technique, we demonstrate that although synapse number and molecular architecture appear essentially intact, RIM-BP2 is necessary for proper coclustering of the P/Q-type Ca_V subunit $Ca_V2.1$ with the AZ protein Bassoon at hippocampal CA3-CA1 synapses. We hypothesize that the observed change in Ca_V localization causes a discrete alteration in the coupling of Ca^{2+} influx and exocytosis, and thereby modifies release probability and, consequently, STP. Additional deletion of RIM-BP1 did not strengthen

Significance

Highly regulated and precise positioning of Ca^{2+} channels at the active zone (AZ) controls Ca^{2+} nanodomains at release sites. Their exact localization affects vesicular release probability (P_{VR}) and is important for proper synaptic transmission during repetitive stimulation. We provide a detailed analysis of synaptic transmission combined with superresolution imaging of the AZ organization in mouse hippocampal synapses lacking Rab-interacting molecule-binding protein 2 (RIM-BP2). By dual- and triple-channel time-gated stimulated emission depletion (gSTED) microscopy, we directly show that RIM-BP2 fine-tunes voltage-gated Ca^{2+} channel 2.1 ($Ca_V2.1$) localization at the AZ. We reveal that RIM-BP2 likely regulates the Ca^{2+} nanodomain by positioning $Ca_V2.1$ channels close to synaptic vesicle release sites. Loss of RIM-BP2 reduces P_{VR} and alters short-term plasticity.

Author contributions: M.K.G., M.M., S.R.-A., B.J.E., V.H., D.S., S.J.S., and C.R. designed research; M.K.G., M.M., S.R.-A., C.G.W., M.M.B., T.T., T.R., M.P., G.V., A.S., and B.R.R. performed research; A.M.W. contributed new reagents/analytic tools; M.K.G., M.M., S.R.-A., C.G.W., M.M.B., T.T., T.R., M.P., and B.R.R. analyzed data; A.M.W. provided data discussion; and M.K.G., M.M., S.R.-A., V.H., D.S., S.J.S., and C.R. wrote the paper.

The authors declare no conflict of interest.

This article is a PNAS Direct Submission.

Freely available online through the PNAS open access option.

[1]M.K.G., M.M., and S.R.-A. contributed equally to this work.

[2]To whom correspondence may be addressed. Email: christian.rosenmund@charite.de, dietmar.schmitz@charite.de, or stephan.sigrist@fu-berlin.de.

This article contains supporting information online at www.pnas.org/lookup/suppl/doi:10.1073/pnas.1605256113/-/DCSupplemental.

the changes in short-term facilitation, supporting our hypothesis that RIM-BP2 is the major RIM-BP paralog at glutamatergic hippocampal synapses.

Results

RIM-BP2 Localization at the AZ of Hippocampal CA3-CA1 Synapses. STED microscopy revealed that DRBP localizes close to the membrane near the AZ center of *Drosophila* NMJ synapses (6), but comparable studies on RIM-BPs at mammalian AZs with nanometer scale resolution are lacking. Quantitative real-time PCR suggested that RIM-BP2 is the predominant paralog in cultured hippocampal neurons (Fig. S1*A*). We analyzed the spatial relationship between RIM-BP2 and two AZ components, Bassoon and MUNC13-1, at CA3-CA1 hippocampal synapses of mouse brain cryosections. On the confocal level, RIM-BP2 colocalized with both AZ proteins (Fig. S1*B*). To dissect the AZ nanoscale architecture, we established triple-channel gSTED with a lateral resolution of ~50 nm in all three channels (Fig. 1*A* and Fig. S1 *B–D*). Analysis of the mean distance between nearest neighbors (*k*-nearest neighbor analysis) revealed that RIM-BP2 is localized at a short distance to Bassoon and MUNC13-1, whereas MUNC13-1 is equidistant to RIM-BP2 and Bassoon ($k = 1$). In coimmunoprecipitations from P2 fractions of mouse brains, RIM-BP2 coprecipitated with RIM and Munc13-1, but not with the Arf GTPase-activating protein GIT, a binding partner of Piccolo (9) and of endocytotic proteins such as Dynamin1 (Fig. S1*E*) and Stonin 2 (10). Together, these results indicate that RIM-BP2 is part of the presynaptic AZ scaffold and forms a complex with the priming factors RIM and Munc13-1.

Generation of a RIM-BP2 Constitutive Knockout Mouse Line. We generated knockout (KO) mice constitutively lacking RIM-BP2 by deleting exon 17 of the RIM-BP2 gene that encodes part of the second SH3 domain (Fig. S2*A*). RIM-BP2–deficient mice were born at Mendelian ratios (Fig. S2*B*) and survived into adulthood. Complete loss of RIM-BP2 protein expression in KO animals was confirmed by immunostaining of hippocampal cryosections (Fig. S2*C*) and immunoblot analysis of P2 fractions using two antibodies targeting different RIM-BP2 epitopes (Fig. S2 *D* and *F*). The expression of other presynaptic proteins such as RIM1/2, MUNC13-1, Erc1b/2, Synaptophysin1, and Synapsin1 was unaltered (Fig. S2 *D* and *E*). Transmission electron microscopy showed that the ultrastructure of the presynaptic AZ was not grossly altered by the absence of RIM-BP2 (Fig. S2 *G–I*).

RIM-BP2 Deletion Moderately Decreases Vesicular Release Probability and Leads to Increased Short-Term Facilitation in Cultured Neurons. To investigate the role of RIM-BP2 in synaptic transmission, we analyzed basic synaptic properties and STP in autaptic hippocampal glutamatergic neurons from RIM-BP2 WT and KO mice. Evoked excitatory postsynaptic current (EPSC) amplitudes were decreased by 20% in RIM-BP2 KO neurons compared with WT (Fig. 1*B*). We further analyzed the coefficient of variation (C.V.) of EPSCs as a measure for the reliability of evoked release. Consistent with previous results from RIM-BP1/2 double KOs (DKOs) (8), we found an increased C.V. in RIM-BP2 KO neurons (Fig. 1*C*). The size of the readily releasable pool (RRP) (11) was not significantly altered (Fig. 1*D*). The probability of a synaptic vesicle being released by an AP [vesicular release probability (P_{VR})] was calculated as the ratio of the EPSC and the RRP charge. P_{VR} was reduced by 10% in RIM-BP2 KO neurons (Fig. 1*E*). Additionally, we assessed release probability (P_R) by monitoring the progressive block of the NMDA receptor-mediated component of the EPSC by the noncompetitive NMDA receptor blocker (5*S*,10*R*)-(+)-5-methyl-10,11-dihydro-5*H*-dibenzo[*a*,*d*] cyclohepten-5,10-imine maleate (MK-801). The block rate, which is proportional to P_R (12), was indeed decreased by ~18% in RIM-BP2 KO neurons (Fig. S3 *A–C*). Spontaneous miniature release, in contrast, was unaltered (Fig. 1 *F* and *G*).

We next investigated how STP is affected by loss of RIM-BP2. Autaptic RIM-BP2 KO neurons showed a robust increase in paired-pulse ratio (PPR) when stimulated with pairs of APs at different interstimulus intervals (ISIs) compared with WT neurons

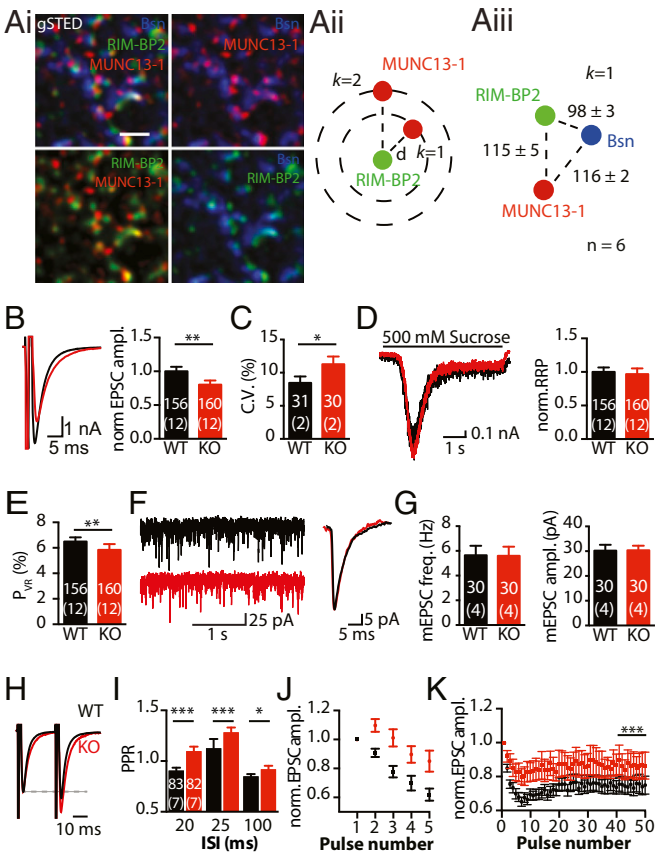

Fig. 1. RIM-BP2 localization at the hippocampal AZ, and effect of RIM-BP2 deletion on synaptic transmission in autaptic hippocampal neurons. (*A*, *i–iii*) Spatial organization of RIM-BP2 in relation to Bassoon (Bsn) and MUNC13-1 at the AZ of CA3-CA1 synapses in WT mouse brain cryosections imaged by gSTED and analyzed using the mean *k*-nearest neighbor distance between clusters. (Scale bar: 500 nm.) (*B*) EPSCs evoked by 2-ms somatic depolarization in RIM-BP2 WT (black) and KO (red) autaptic neurons. Amplitudes (ampl.) were normalized (norm.) to WT mean of the same culture. (*C*) C.V.s of 24 EPSC amplitudes recorded during a period of 2 min. (*D*) Synaptic responses to application of hypertonic sucrose (500 mM) solution probing the RRP. (*E*) P_{VR} of the same cells as in *B* and *D*. (*F*) Spontaneous release and averages of miniature EPSCs (mEPSCs) from the same cells. (G) mEPSC amplitudes and frequencies (freq.). (*H*) Normalized traces of two EPSCs at an ISI of 25 ms. (*I*) PPR calculated for the indicated ISIs. Normalized amplitudes of the same cells as in *I* in response to 5 APs triggered at 50 Hz (*J*) or 50 APs at 10 Hz (*K*). The last 10 EPSCs of the 10-Hz train are larger in KO neurons compared with WT. The numbers of neurons and independent cultures analyzed are shown within the bars. Data are expressed as mean ± SEM. **P* < 0.05; ***P* < 0.01; ****P* < 0.001.

(Fig. 1 *H* and *I*). During short bursts of five APs at 50 Hz (Fig. 1*J*), EPSCs showed initial facilitation, followed by moderate depression in RIM-BP2 KO neurons but significant depression in WT neurons. Similarly, RIM-BP2 KO neurons exhibited significantly reduced depression of EPSC amplitudes during 10-Hz trains compared with WT neurons (Fig. 1*K*).

RIM-BP2 Deletion Alters STP in Acute Hippocampal Slices. To verify the results independently in autaptic culture, we analyzed synaptic transmission in the CA1 area of acute hippocampal slices. The input/output function relating field recordings of excitatory postsynaptic potentials (fEPSPs) and fiber volley amplitudes were unchanged (Fig. 2*A*), suggesting that the loss of RIM-BP2 does not cause major alterations in basal synaptic transmission.

However, the PPR of fEPSPs was significantly elevated for all ISIs (Fig. 2 *B* and *C*), corroborating the cell culture results. Train stimulations with 25 pulses at 14 Hz caused greater initial facilitation and

less depression of fEPSPs in RIM-BP2 KO compared with WT mice (Fig. 2*D*). As in autaptic cultures, spontaneous miniature release was unaltered in hippocampal slices (Fig. 2*E*). Together, the data from acute slices and autaptic culture demonstrate enhanced short-term facilitation in the absence of RIM-BP2.

Additional RIM-BP1 Deletion Does Not Exacerbate the RIM-BP2 KO Phenotype. We crossed RIM-BP2 KO mice with constitutive RIM-BP1 KO mice (Fig. S4 *A*–*F*) to generate RIM-BP1/2 DKO mice. In area CA1 of acute hippocampal slices, input/output functions of RIM-BP2 KO and RIM-BP1/2 DKO were indistinguishable (Fig. S4*G*). We then compared PPRs (Fig. S4*H*) and STP (Fig. S4*I*) in RIM-BP2 single-KO and RIM-BP1/2 DKO slices. Additional deletion of RIM-BP1 did not exacerbate the increased facilitation observed in the single RIM-BP2 KO. Thus, our data support the hypothesis that RIM-BP2 is the major RIM-BP paralog in murine hippocampal neurons.

RIM-BP2 Deletion Does Not Affect Vesicle Priming or Replenishment. RIM and Munc13 are known to mediate priming of synaptic vesicles (1, 13). Thus, could the increased short-term facilitation be caused by RIM-BP2 modulating priming through its interactions with the RIM/Munc13-1 complex? We can exclude this possibility for several reasons. First, the unaltered spontaneous release (Figs. 1*G* and 2*E* and Fig. S3*G*) argues against a priming defect in RIM-BP2 KO synapses (14). Second, the transmitter release induced by subsaturating hypertonic stimulation (250 mM sucrose) compared with release induced by a saturating stimulus (500 mM sucrose) was identical in autaptic RIM-BP2 WT and KO neurons, indicating no difference in vesicle fusogenicity (14) (Fig. S3 *D* and *E*). Third, due to a higher energy barrier for fusion, sucrose-induced release kinetics would be slower in the case of a priming deficit (15). However, peak release rates were unchanged (Fig. S3*F*). Additionally, we tested recovery from pool depletion but did not detect any difference between WT and RIM-BP2 KO neurons (Fig. S3 *H* and *I*), suggesting that RIM-BP2 deletion does not affect RRP replenishment.

RIM-BP2 Deletion Alters Ca^{2+} Sensitivity of Release. Work at *Drosophila* NMJ synapses demonstrated that deletion of DRBP results in defective Ca_V localization, reduced Ca^{2+} influx, impaired synaptic transmission, and increased short-term facilitation (6). We examined presynaptic Ca^{2+} influx in cultured hippocampal neurons using the fast Ca^{2+} sensor GCamp6f coupled to synaptophysin (SynGCamp6f) that specifically localizes the sensor to the presynapse (Fig. 3*A*). We did not detect significant differences in global Ca^{2+} signals in response to two (at 20 Hz) or 50 (at 10 Hz) APs (Fig. 3 *B* and *C*). Furthermore, we analyzed the dependence of transmitter release on varying external Ca^{2+} concentrations ($[Ca^{2+}]_{ext}$s) in RIM-BP2 WT and KO autaptic neurons in detail (Fig. 3 *D* and *E*). The relative sensitivity of EPSC amplitudes to varying $[Ca^{2+}]_{ext}$s (0.5–10 mM Ca^{2+}/1 mM Mg^{2+}) was determined by intermittent measurements of EPSC amplitudes from control solution (2 mM Ca^{2+}/4 mM Mg^{2+}; Fig. 3*D*). Normalizing to control EPSCs, we found that the relative potentiation of release is increased in RIM-BP2 KO at 4 mM and 10 mM $[Ca^{2+}]_{ext}$s (Fig. 3*E*, *Left*). To fit a Hill function, we normalized the same dataset to saturating 10 mM $[Ca^{2+}]_{ext}$, resulting in almost identical Ca^{2+} dose–response curves for WT and KO neurons (Fig. 3*E*, *Right*), suggesting no change in the Ca^{2+} cooperativity *n* for release and similar numbers of Ca_Vs at the AZ of both genotypes. These findings, however, do not exclude changes in residual Ca^{2+} at local micro- or nanodomains in the RIM-BP2 KO.

We next determined PPRs at different $[Ca^{2+}]_{ext}$s (Fig. 3*F*). In 0.5–2 mM $[Ca^{2+}]_{ext}$, PPRs (25-ms ISI) were significantly increased in RIM-BP2 KO neurons, whereas PPRs were indistinguishable in 4–10 mM $[Ca^{2+}]_{ext}$. In a second set of experiments, we analyzed PPRs at different ISIs (25–250 ms) and found similar results for all chosen ISIs (Fig. S3*J*). PPRs were significantly increased in lower $[Ca^{2+}]_{ext}$s (≤2 mM) and also for ISIs up to 250 ms with the exception of 0.5 mM $[Ca^{2+}]_{ext}$, where PPRs at 100 ms and 250 ms were identical in WT and RIM-BP2 KO. Overall, the differences in PPRs became smaller with increasing $[Ca^{2+}]_{ext}$. At 4 mM $[Ca^{2+}]_{ext}$, only the PPR values recorded at 50-ms and 250-ms ISIs were significantly increased in RIM-BP2 KO neurons.

We also measured P_{VR} at low and high $[Ca^{2+}]_{ext}$s and found that in 0.5 mM $[Ca^{2+}]_{ext}$, P_{VR} was reduced by 21% in RIM-BP2 KO neurons (Fig. 3*G*), whereas the difference in 4 mM $[Ca^{2+}]_{ext}$ was not significant. Similarly, RIM-BP2 KO had significantly reduced

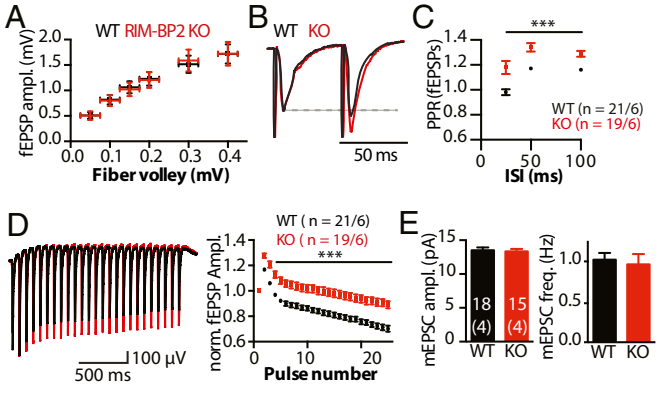

Fig. 2. RIM-BP2 deletion alters STP in acute hippocampal slices. (*A*) Input/output curves relating the amplitude of the presynaptic fiber volley to the fEPSP amplitude in the stratum radiatum of area CA1 of acute hippocampal slices at different stimulus intensities (0.05 mV–0.2 mV: WT, $n = 21$; KO, $n = 19$; 0.3 mV: WT, $n = 18$; KO, $n = 14$; 0.4 mV: WT, $n = 16$; KO, $n = 13$). (*B*) Normalized fEPSPs in response to a paired pulse with 50-ms ISI. (*C*) PPRs of fEPSPs at different ISIs. (*D*) fEPSPs elicited by a 14-Hz stimulation train, with stimulation artifacts blanked for better visibility. (*E*) mEPSC amplitudes and frequencies recorded from CA1 pyramidal neurons. The numbers of slices and independent animals are indicated. Data are expressed as mean ± SEM. ***$P < 0.001$.

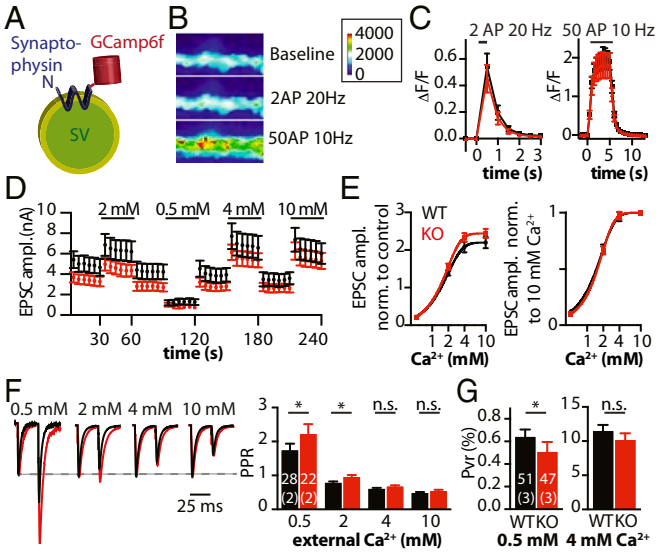

Fig. 3. RIM-BP2 deletion alters Ca^{2+} sensitivity of release. (*A*) Schematic representation of the genetically encoded Ca^{2+} indicator synGCamp6f at the membrane of a synaptic vesicle. Heat-colored images of a WT dendrite (*B*) and quantification of synGCamp6f fluorescence change (ΔF/F) during stimulation with two APs at 20 Hz and 50 APs at 10 Hz (*C*). (*D*) Mean EPSCs of WT (black) and RIM-BP2 KO (red) autaptic neurons in different $[Ca^{2+}]_{ext}$s. The $[Ca^{2+}]_{ext}$s of test solutions are indicated (all 1 mM Mg^{2+}). A control solution (2 mM Ca^{2+}/4 mM Mg^{2+}) was applied in between. (*E*) EPSC amplitudes at different $[Ca^{2+}]_{ext}$s normalized to alternating control responses (*Left*) and to 10 mM $[Ca^{2+}]_{ext}$ (*Right*). Hill functions were fitted to the data. (*F*) Normalized EPSCs in response to a paired stimulus and mean PPRs at indicated $[Ca^{2+}]_{ext}$s. (*G*) P_{VR} of autaptic hippocampal neurons in 0.5 mM and 4 mM $[Ca^{2+}]_{ext}$s. The numbers of neurons and independent cultures analyzed are shown within the bars. Data are expressed as mean ± SEM. *$P < 0.05$. n.s., not significant.

EPSC amplitudes, accompanied by an increased C.V. of the EPSCs in low, but not high, $[Ca^{2+}]_{ext}$ (Fig. S3*K*).

Altogether, these data show that loss of RIM-BP2 leads to an impairment of Ca^{2+}-secretion coupling that can be overcome by elevating $[Ca^{2+}]_{ext}$.

RIM-BP2 KO Alters Presynaptic $Ca_V2.1$ Channel Localization. If priming, global presynaptic Ca^{2+} influx, and Ca^{2+} cooperativity are unaltered in the RIM-BP2 KO neurons, could altered Ca_V positioning explain the changes in release probability and PPR?

To address this question, we turned to superresolution microscopy and tested if deletion of RIM-BP2 alters the subsynaptic positioning of the P/Q-type Ca_V subunit $Ca_V2.1$, because interference with RIM-BP2 and Bassoon interaction affects their synaptic localization (5). We first measured the synaptic distribution of $Ca_V2.1$s in relation to the AZ protein Bassoon in the stratum radiatum of the hippocampal area CA1 of WT and RIM-BP2 KO mice by dual-channel gSTED (Fig. 4 *A*–*F*). We found that loss of RIM-BP2 did not significantly affect either the total number of $Ca_V2.1$ and Bassoon clusters or their ratio (Fig. S5 *A* and *B*), in agreement with the unaltered total Ca^{2+} influx observed by Ca^{2+} imaging (Fig. 3 *A*–*C*). Notably, however, the average number of Bassoon clusters at short distance intervals from $Ca_V2.1$ clusters was significantly reduced by more than 30% (Fig. 4 *B*, *i* and *C*). This finding indicates that RIM-BP2 deletion alters $Ca_V2.1$ localization at short distances from the AZ. This effect is not due to an overall change in total cluster number. Supporting these results, at RIM BP2 KO synapses, we observed a 50% increase in the mean *k* distance of Bassoon clusters surrounding a given $Ca_V2.1$ cluster, but the *P* value reached was only 0.068 ($k = 1$; Fig. 4 *B*, *ii* and *D*). The mean *k* distance between individual Bassoon clusters did not significantly change in the absence of RIM-BP2, suggesting that although the distance between single AZs is unaltered in RIM-BP2 KO mice, $Ca_V2.1$s are localized more distal from the AZ (Fig. 4 *E* and *F*).

To map $Ca_V2.1$ localization precisely relative to the AZ protein RIM1 and the postsynaptic marker Homer1, we established triple-channel gSTED (Fig. 4 *G*–*N*). The total number of $Ca_V2.1$, RIM1, and Homer1 clusters did not significantly differ between WT and RIM-BP2 KO (Fig. S5 *C*–*E*). However, RIM-BP2 KO mice showed higher variability in RIM1 cluster number as expressed in a highly variable RIM1/$Ca_V2.1$ ratio (Fig. S5 *D* and *E*). This

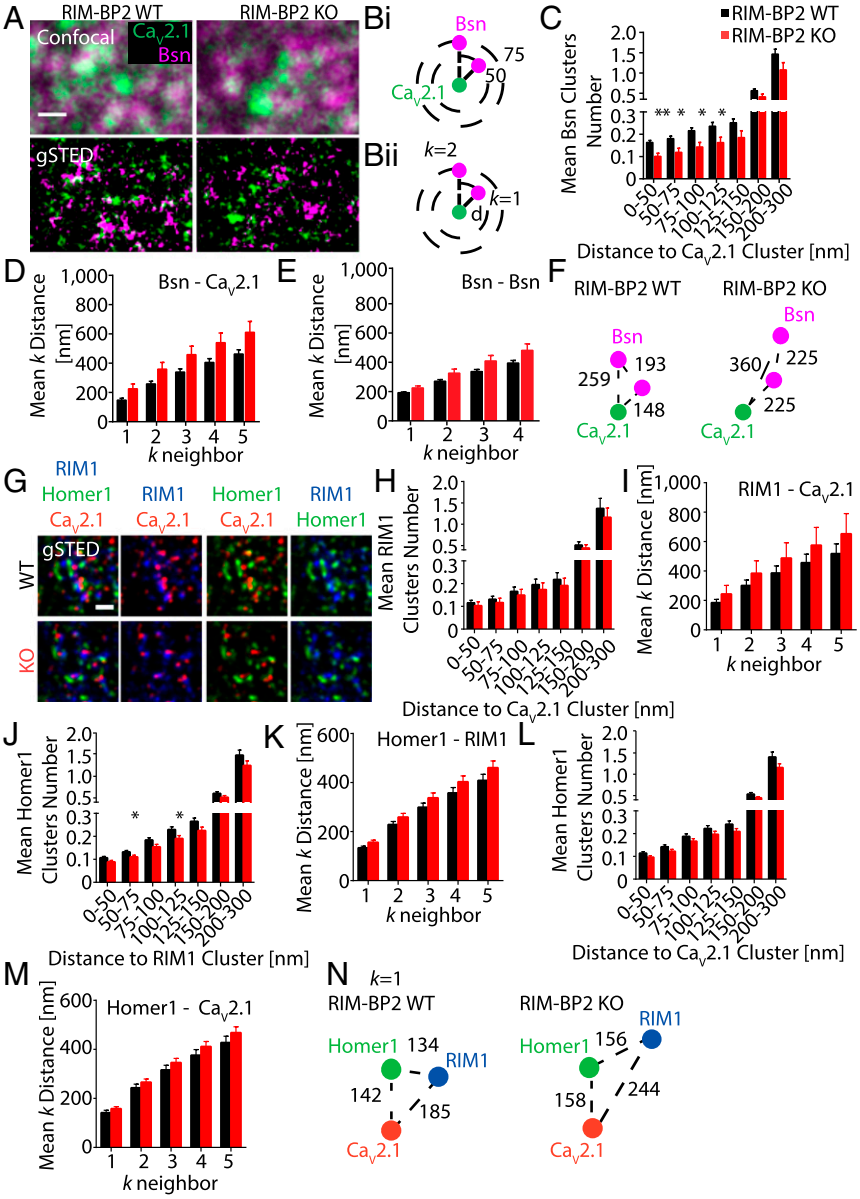

Fig. 4. RIM-BP2 loss results in defective $Ca_V2.1$ clustering at the AZ. (*A*) $Ca_V2.1$ and Bsn clusters imaged in situ at CA3-CA1 hippocampal synapses of RIM-BP2 WT and KO mice by dual-channel gSTED (*Bottom*) compared with confocal acquisition (*Top*). (*B*) Schematic representation of two kinds of cluster analysis. (*B*, *i*) Bsn clusters within indicated sampling distances (e.g., 50 nm, 75 nm) to a given $Ca_V2.1$ cluster were quantified and averaged on thousands of $Ca_V2.1$ clusters per image. (*B*, *ii*) Mean distance between the *k*-nearest neighbor Bsn cluster and $Ca_V2.1$ cluster ($k = 1$, $k = 2$, $k = 3$, $k = 4$, $k = 5$). (*C*) Bsn cluster numbers at short distances from $Ca_V2.1$ clusters (WT, $n = 5$; KO, $n = 6$). (*D*–*F*) Mean *k* distance between Bsn and $Ca_V2.1$ clusters (*D*) and between neighboring Bsn clusters (*E*) in RIM-BP2 KO mice. (*G*) Triple-channel gSTED images of $Ca_V2.1$, RIM1, and Homer1 at CA3-CA1 hippocampal synapses (WT, $n = 9$; KO, $n = 9$). (*H*) RIM1 clusters found in proximity to $Ca_V2.1$ channels. (*I*) Mean *k* distance of RIM1 clusters to $Ca_V2.1$ clusters. Homer1-RIM1 clustering (*J*) and Homer1-RIM1 mean *k* distance (*K*). Homer1 clusters close to $Ca_V2.1$ channels (*L*), and mean *k* distances between Homer1 clusters and $Ca_V2.1$ (*M*) are shown. (*N*) $Ca_V2.1$ spatial organization relative to RIM1 and Homer1 at excitatory hippocampal synapses. (Scale bars: *A* and *G*, 500 nm.) Distances between clusters are represented in nanometers. Values are expressed as mean ± SEM. $*P < 0.05$; $**P < 0.01$.

variability did not affect net RIM1 clustering relative to $Ca_V2.1$s, although we also observed a trend here toward increased mean k distance of RIM1 surrounding $Ca_V2.1$ clusters (Fig. 4 *H* and *I*). We also found a significantly reduced mean number of Homer1 clusters surrounding a given RIM1 cluster at 50–75 nm and 100–125 nm in RIM-BP2 KO (Fig. 4*J*), suggesting an effect of RIM-BP2 on RIM1 clustering. However, the mean k distance of neighboring Homer1 toward RIM1 clusters did not significantly change (Fig. 4*K*). These data indicate that RIM-BP2 might exert a minor effect on the exact RIM1 spatial distribution at the AZ. The mean number of Homer1 clusters relative to $Ca_V2.1$ was not altered in RIM-BP2 KO (Fig. 4*L*). At RIM-BP2 WT synapses, the closest neighboring Homer1 cluster was found at 142 ± 10 nm from $Ca_V2.1$ clusters (Fig. 4 *M* and *N*). In RIM-BP2 KO, this distance increased by 11% with a statistical P value at the edge of significance ($P = 0.05$), demonstrating that RIM-BP2 deletion does not grossly alter $Ca_V2.1$ positioning versus the postsynaptic density.

Our structural analysis shows that loss of RIM-BP2 modifies the molecular architecture of the AZ by changing the relative distribution of $Ca_V2.1$s versus the AZ scaffold protein Bassoon. Increased distance should result in a larger functional coupling distance between the Ca^{2+} channel and Ca^{2+} sensor, and therefore a stronger effect of the slow Ca^{2+} chelator EGTA (16). Thus, we tested whether application of the membrane-permeable EGTA acetoxymethyl ester (EGTA-AM) would have differential effects on EPSC amplitudes and P_{VR} of WT and RIM-BP2 KO autaptic neurons (Fig. S6 *A–C*). Indeed, preincubation with 25 μM EGTA-AM decreased EPSC amplitudes more in RIM-BP2 KO than in WT (Fig. S6*A*). Although this effect was not statistically significant, EGTA-AM did reduce P_{VR} by more than 50% in RIM-BP2 KO without altering WT P_{VR} (Fig. S6*B*). Thus, together with our structural data, the EGTA-AM effect on P_{VR} in RIM-BP2 KO neurons supports the idea of a larger distance between Ca^{2+} channels and Ca^{2+} sensors at release sites in the absence of RIM-BP2. Our analysis provides evidence that RIM-BP2 contributes to proper positioning of $Ca_V2.1$s at AZs of hippocampal glutamatergic synapses that allows precise Ca^{2+}-secretion coupling.

Discussion

Presynaptic neurotransmitter release is a highly orchestrated process ensuring high-fidelity neuronal communication. The RIM/RIM-BP complex has been implicated in enhancing the efficiency of the fusion machinery and the positioning of synaptic vesicles in close proximity to Ca_Vs to optimize Ca^{2+}-secretion coupling (2, 5, 6). Recently, Acuna et al. (8) showed that deletion of RIM-BP1 and RIM-BP2 in the murine Calyx of Held impairs the reliability of evoked neurotransmitter release, presumably due to an uncoupling of Ca_Vs from release sites. At the *Drosophila* NMJ, the RIM-BP ortholog DRBP, together with Bruchpilot, is an AZ core component, and elimination of DRBP causes severe structural deficits in AZ organization, associated with strongly impaired basal transmission and STP (6, 7).

Our analysis of the RIM-BP2 KO in glutamatergic hippocampal neurons revealed a moderate disruption of the AZ architecture in comparison to the *Drosophila* phenotype, resulting in a mild decrease in release efficiency but a pronounced alteration in STP. Thus, rather subtle modifications in the fine positioning of the Ca_Vs within the AZ are sufficient to promote changes in release probability and induce robust STP alterations.

The altered P_{VR}, PPR, and STP of RIM-BP2–deficient neurons are most plausibly explained by changes in the nanoscale organization of protein architectures within the AZs (i.e., the mislocalization of $Ca_V2.1$s in proximity to Bassoon). We interpret these results as an indication of increased coupling distances between Ca^{2+} channels and release sites, also based on our EGTA-AM experiments. These data are also consistent with previously published results (5, 8). A larger distance between $Ca_V2.1$s and release sites would result in an altered local Ca^{2+} profile "seen" by the Ca^{2+} sensor for release, which determines vesicle fusion and strongly depends on the coupling distance (17). RIM-BPs have been identified in a number of studies as candidate genes for autism spectrum disorder (ASD) (18–21). Although neurons might be able to compensate for the 10% decrease in P_{VR} by homeostatic mechanisms, it is likely that the robust changes in STP might ultimately severely alter the computational properties and function of the affected neuronal networks, and thereby perturb synaptic information processing (22).

It should be noted that a very similar phenotype with mildly reduced P_{VR} and robustly increased short-term facilitation is also evident in Ras-related protein Rab3-deficient neurons (23). Schlüter et al. (23) speculate that Rab3 "superprimes" a subset of vesicles, specifically increasing their release probability. One possible mechanism is that Rab3 directs vesicles to release sites closer to Ca^{2+} channels, where they would have an intrinsically higher release probability. This scenario might explain the similarities in both phenotypes. Whereas Rab3 would control coupling of synaptic vesicles and Ca^{2+} channels from the vesicle side, RIM-BP2 might act from the Ca^{2+} channel side in a subset of AZs. Indeed, in our analysis, we see only a relatively small fraction of AZs having a $Ca_V2.1$ within 125 nm. At this subset of AZs, proper $Ca_V2.1$ localization depends on RIM-BP2.

We established triple-channel gSTED to determine precise distances between clusters of specific synaptic components at CA3-CA1 synapses in situ. At other excitatory synapses, previous studies using direct stochastical optical reconstruction microscopy (dSTORM) reported a Bassoon-Homer1 average axial distance of 154 nm (24). Accordingly, we find that at WT synapses, Homer1 is located at 142 nm and 134 nm from $Ca_V2.1$ and RIM1, respectively, indicating that gSTED can be used reliably to map protein cluster localization, and thus synaptic substructures at mammalian synapses in situ. However, with both superresolution techniques, true cluster distances are obviously influenced by using indirect immunolabeling, because the size of the primary/secondary IgG sandwich (~20 nm) and the position of the epitopes recognized by the antibodies likely influence the exact measured distances (epitopes targeted by each antibody are listed in Table S1). Still, comparing the values between mutant and WT constellation should be meaningful.

Here, we show that at hippocampal CA3-CA1 AZs, RIM-BP2 is located close to Bassoon and Munc13-1 in a complex in which each nearest neighbor is rather equidistant (~100 nm). According to ultrastructural studies, cortical pyramidal neuron synapses usually have a single AZ with a highly variable area of about 0.04 μm^2 (25, 26). Our cluster analysis at CA3-CA1 synapses maps two adjacent Bassoon clusters at less than 200 nm. We therefore assume that the first ($k = 1$) nearest neighbor of our analysis might indicate a neighboring cluster within a single AZ. To address this point more precisely, 3D reconstruction of AZ components imaged at sub-diffraction axial resolution will be necessary. Our data also show that the localization of $Ca_V2.1$ in close apposition to the PSD marker Homer1 is relatively stable even in the absence of RIM-BP2. Although the overall RIM1 expression level was not affected in crude synaptosomal membranes, we observed increased variability in RIM1 total cluster number in RIM-BP2–deficient synapses. This increased variability may reflect altered nanoscale distribution of RIM1 localization within AZs and toward the postsynapse, which is supported by a trend toward a larger RIM1-to-$Ca_V2.1$ mean k distance and slightly, but significantly, altered Homer1 clustering relative to RIM1 in RIM-BP2 KO.

We performed a detailed analysis of RIM-BP2 loss of function mostly in autaptic neurons, whereas our structural analysis was done in situ to provide information on the organization of the AZ within the hippocampus. Nevertheless, our PPR and STP experiments in slices demonstrate that RIM-BP2 KO results in a similar functional defect in both preparations. On the other hand, our EGTA-AM experiments provide evidence that RIM-BP2 is necessary for proper Ca^{2+} channel localization at the AZ also in vitro.

Besides coupling of Ca_Vs to release sites, other functions have been suggested for RIM-BPs. At the *Drosophila* NMJ, DRBP is required for homeostatic modulation of presynaptic Ca^{2+} influx and the size of the RRP, as well for as recovery from pool depletion (7). In contrast, at the murine Calyx of Held, RRP size and the kinetics of priming into the RRP are not RIM-BP–dependent

(8). However, the release of the RRP was significantly decelerated in RIM-BP1/2 DKO. In our autaptic culture system, we observed no differences in RRP size, fusogenicity, or peak release rates, and we did not detect changes in the recovery from pool depletion. These results suggest that loss of RIM-BPs manifests distinctively at different specialized synapse types.

Why are the effects of RIM-BP2 deletion on presynaptic structure and function of hippocampal synapses rather subtle compared with the severe phenotype at *Drosophila* NMJ AZs? Differences in the exact structure of the AZ scaffolds and the level of genetic redundancy might well be involved here. In fact, different isoforms of AZ proteins likely contribute to shaping specific functions that differ from synapse to synapse. For both hippocampal and NMJ synapses, however, the RIM/RIM-BP complex is crucial for precise Ca_V localization at the AZ and expression of STP and/or long-term plasticity. The comparison of KO phenotypes suggests that in *Drosophila*, DRBP plays a more pivotal role (6, 27), whereas judged from single gene KOs at mammalian synapses, RIM is functionally most important (1, 2, 8, 28–30). Still, the importance of RIM-BPs for STP is conserved between flies and mammals (6, 8, 31), consistent with the highly conserved molecular interactions between RIM-BPs, Ca_Vs, and RIM (2, 4, 6).

Further investigation is required to understand fully the molecular role of RIM-BPs in different synapse types, which might also depend on the type of presynaptic Ca_V present. Studying potential behavioral deficits in RIM-BP1 and RIM-BP2 KO mice and the function of RIM-BPs in neuronal circuits implicated in ASD (32) will likely advance our understanding of how the disruption of RIM-BP function might lead to behavioral and cognitive deficits.

Methods

KO Mouse Generation. RIM-BP2 and RIM-BP1 targeting vector construction and KO mouse generation by standard homologous recombination were performed by genOway. All animal experiments were approved by the animal welfare committee of Charité Universitätsmedizin Berlin and the Landesamt für Gesundheit und Soziales Berlin.

Cell Culture and Electrophysiological Recordings. Primary neuronal cultures were prepared as described by Arancillo et al. (14). Whole-cell patch-clamp recordings in autaptic neurons were performed at days in vitro 13–21 as described (14).

Slice Preparation and Electrophysiological Recordings. Acute hippocampal slices were prepared as described by Stempel et al. (33). The 300-μm-thick horizontal slices were maintained for 30 min at 35 °C in sucrose-artificial cerebrospinal fluid (ACSF) and subsequently stored in ACSF at room temperature. Experiments were started after 30 min and no longer than 6 h after preparation. A detailed description of electrophysiological experiments is provided in *SI Methods*.

Immunohistochemical Analysis and gSTED Imaging. Following immunostaining, sagittal cryosections (10 μm) of RIM-BP2 WT and KO brains were imaged by gSTED with a Leica SP8 gSTED microscope (Leica Microsystems) equipped with two depletion lasers (592 nm and 775 nm). Cluster analysis on deconvolved images was performed with Amira (Visualization Sciences Group) and a MATLAB (The MathWorks, Inc.) custom-written script.

SynGCamp6f Imaging. SynGCamp6f was generated analogous to synGCamp2 (34) by fusing GCamp6f (35) to the C terminus of the synaptic vesicle protein synaptophysin. Imaging was done as previously described (34).

SI Methods contains figures, a detailed description of the methods used, antibodies (Table S1), raw values, and statistical analysis (Tables S2–S4).

ACKNOWLEDGMENTS. We thank Annegret Felies, Berit Soehl-Kielczynski, Sabine Lenz, Katja Poetschke, Carola Schweynoch, Rike Dannenberg, and Bettina Brokowski for technical support; and Lauren Mamer for discussions. We thank Burkhard Wiesner and Martin Lehmann (FMP cellular imaging facility) for the use of the Leica gSTED microscope and for the fluorescent beads; Andreas Grasskamp for the point spread function estimation by Gaussian fit; Anna Fejtova and Eckart Gundelfinger for the RIM-BP2 antibody; and Pietro De Camilli for the Dynamin1 antibody. This work was supported by the Deutsche Forschungsgemeinschaft (Collaborative Research Grant SFB 958 [to V.H. (A1, A7), D.S. (A5), S.S. (A3, A6), C.R. (A5)] and Emmy-Noether Program (to A.M.W.), Studienstiftung des deutschen Volkes PhD Fellowship (to M.K.G.), and Excellence Cluster Neurocure Exc257 (to B.J.E., V.H., D.S., S.S., and C.R.).

1. Deng L, Kaeser PS, Xu W, Südhof TC (2011) RIM proteins activate vesicle priming by reversing autoinhibitory homodimerization of Munc13. *Neuron* 69(2):317–331.
2. Kaeser PS, et al. (2011) RIM proteins tether Ca2+ channels to presynaptic active zones via a direct PDZ-domain interaction. *Cell* 144(2):282–295.
3. Wang Y, Sugita S, Sudhof TC (2000) The RIM/NIM family of neuronal C2 domain proteins. Interactions with Rab3 and a new class of Src homology 3 domain proteins. *J Biol Chem* 275(26):20033–20044.
4. Hibino H, et al. (2002) RIM binding proteins (RBPs) couple Rab3-interacting molecules (RIMs) to voltage-gated Ca(2+) channels. *Neuron* 34(3):411–423.
5. Davydova D, et al. (2014) Bassoon specifically controls presynaptic P/Q-type Ca(2+) channels via RIM-binding protein. *Neuron* 82(1):181–194.
6. Liu KSY, et al. (2011) RIM-binding protein, a central part of the active zone, is essential for neurotransmitter release. *Science* 334(6062):1565–1569.
7. Müller M, Genç Ö, Davis GW (2015) RIM-binding protein links synaptic homeostasis to the stabilization and replenishment of high release probability vesicles. *Neuron* 85(5):1056–1069.
8. Acuna C, Liu X, Gonzalez A, Südhof TC (2015) RIM-BPs mediate tight coupling of action potentials to Ca(2+)-triggered neurotransmitter release. *Neuron* 87(6):1234–1247.
9. Kim S, et al. (2003) The GIT family of proteins forms multimers and associates with the presynaptic cytomatrix protein Piccolo. *J Biol Chem* 278(8):6291–6300.
10. Podufall J, et al. (2014) A presynaptic role for the cytomatrix protein GIT in synaptic vesicle recycling. *Cell Reports* 7(5):1417–1425.
11. Rosenmund C, Stevens CF (1996) Definition of the readily releasable pool of vesicles at hippocampal synapses. *Neuron* 16(6):1197–1207.
12. Rosenmund C, Clements JD, Westbrook GL (1993) Nonuniform probability of glutamate release at a hippocampal synapse. *Science* 262(5134):754–757.
13. Varoqueaux F, et al. (2002) Total arrest of spontaneous and evoked synaptic transmission but normal synaptogenesis in the absence of Munc13-mediated vesicle priming. *Proc Natl Acad Sci USA* 99(13):9037–9042.
14. Arancillo M, et al. (2013) Titration of Syntaxin1 in mammalian synapses reveals multiple roles in vesicle docking, priming, and release probability. *J Neurosci* 33(42):16698–16714.
15. Basu J, Betz A, Brose N, Rosenmund C (2007) Munc13-1 C1 domain activation lowers the energy barrier for synaptic vesicle fusion. *J Neurosci* 27(5):1200–1210.
16. Eggermann E, Bucurenciu I, Goswami SP, Jonas P (2011) Nanodomain coupling between Ca^{2+} channels and sensors of exocytosis at fast mammalian synapses. *Nat Rev Neurosci* 13(1):7–21.
17. Nadkarni S, Bartol TM, Stevens CF, Sejnowski TJ, Levine H (2012) Short-term plasticity constrains spatial organization of a hippocampal presynaptic terminal. *Proc Natl Acad Sci USA* 109(36):14657–14662.
18. Bucan M, et al. (2009) Genome-wide analyses of exonic copy number variants in a family-based study point to novel autism susceptibility genes. *PLoS Genet* 5(6):e1000536.
19. Pinto D, et al. (2010) Functional impact of global rare copy number variation in autism spectrum disorders. *Nature* 466(7304):368–372.
20. Hussman JP, et al. (2011) A noise-reduction GWAS analysis implicates altered regulation of neurite outgrowth and guidance in autism. *Mol Autism* 2(1):1.
21. Corominas R, et al. (2014) Protein interaction network of alternatively spliced isoforms from brain links genetic risk factors for autism. *Nat Commun* 5:3650.
22. Klyachko VA, Stevens CF (2006) Excitatory and feed-forward inhibitory hippocampal synapses work synergistically as an adaptive filter of natural spike trains. *PLoS Biol* 4(7):e207.
23. Schlüter OM, Basu J, Südhof TC, Rosenmund C (2006) Rab3 superprimes synaptic vesicles for release: Implications for short-term synaptic plasticity. *J Neurosci* 26(4):1239–1246.
24. Dani A, Huang B, Bergan J, Dulac C, Zhuang X (2010) Superresolution imaging of chemical synapses in the brain. *Neuron* 68(5):843–856.
25. Schikorski T, Stevens CF (1997) Quantitative ultrastructural analysis of hippocampal excitatory synapses. *J Neurosci* 17(15):5858–5867.
26. Holderith N, et al. (2012) Release probability of hippocampal glutamatergic terminals scales with the size of the active zone. *Nat Neurosci* 15(7):988–997.
27. Graf ER, et al. (2012) RIM promotes calcium channel accumulation at active zones of the Drosophila neuromuscular junction. *J Neurosci* 32(47):16586–16596.
28. Schoch S, et al. (2002) RIM1α forms a protein scaffold for regulating neurotransmitter release at the active zone. *Nature* 415(6869):321–326.
29. Castillo PE, Schoch S, Schmitz F, Südhof TC, Malenka RC (2002) RIM1α is required for presynaptic long-term potentiation. *Nature* 415(6869):327–330.
30. Kintscher M, Wozny C, Johenning FW, Schmitz D, Breustedt J (2013) Role of RIM1α in short- and long-term synaptic plasticity at cerebellar parallel fibres. *Nat Commun* 4:2392.
31. Müller M, Liu KSY, Sigrist SJ, Davis GW (2012) RIM controls homeostatic plasticity through modulation of the readily-releasable vesicle pool. *J Neurosci* 32(47):16574–16585.
32. Courchesne E, et al. (2007) Mapping early brain development in autism. *Neuron* 56(2):399–413.
33. Stempel AV, et al. (2016) Cannabinoid type 2 receptors mediate a cell type- specific plasticity in the hippocampus. *Neuron* 90(4):795–809.
34. Herman MA, Ackermann F, Trimbuch T, Rosenmund C (2014) Vesicular glutamate transporter expression level affects synaptic vesicle release probability at hippocampal synapses in culture. *J Neurosci* 34(35):11781–11791.
35. Chen T-W, et al. (2013) Ultrasensitive fluorescent proteins for imaging neuronal activity. *Nature* 499(7458):295–300.
36. Watanabe S, et al. (2014) Clathrin regenerates synaptic vesicles from endosomes. *Nature* 515(7526):228–233.
37. Clements JD, Bekkers JM (1997) Detection of spontaneous synaptic events with an optimally scaled template. *Biophys J* 73(1):220–229.
38. Xue M, et al. (2010) Binding of the complexin N terminus to the SNARE complex potentiates synaptic-vesicle fusogenicity. *Nat Struct Mol Biol* 17(5):568–575.